Control-Oriented Thermal Model for a Hybrid Vehicle Battery

Rishit B. Modi

Thesis submitted to the Faculty of the
Virginia Polytechnic Institute and State University
in partial fulfillment of the requirements for the degree of

Master of Science
in
Mechanical Engineering

Douglas J. Nelson, Chair
Alexander Leonessa
Pratap Tokekar

May 11, 2020
Blacksburg, Virginia

Keywords: Lithium-ion batteries, thermal model, heat transfer

Control-Oriented Thermal Model for a Hybrid Vehicle Battery

Rishit B. Modi

(ABSTRACT)

In a bid to reduce vehicular emissions, automobile manufacturers are moving towards electric and hybrid vehicles. Most hybrid vehicles use Lithium-ion batteries as energy storage systems. Lithium-ion batteries have a narrow range of temperature within which they can be operated efficiently. Operation of Lithium-ion batteries outside this range decreases the life of batteries and reduces performance of the vehicle. Due to this limitation, it is important to prevent overheating of Lithium-ion batteries. Battery pack studied in this work has a fan system for air-cooling the cells. The battery management system (BMS) in the battery pack functions to keep the temperature of the cells within allowable limits by either regulating the fan speed or communicating with the vehicle controller to adjust magnitude of applied current. BMS used in the work is equipped with limited number of temperature sensors that can measure surface temperature of few cells in the battery pack. Additional temperature information can be used for better thermal control of the cells in the battery pack. Lithium-ion cells are known to have a measurable temperature gradient when operating under extreme conditions. As a result, the surface temperature of cells as measured by the temperature sensors in BMS is not always representative of the maximum cell temperature. To overcome these limitations, a simplified transient thermal model predicting core and surface temperature of cell is presented in this work. This model can be implemented in a BMS for real-time control of cell temperature. The thermal model is validated against data available from testing the battery pack. Different current profiles, representative of real-world driving scenarios, are applied to the thermal model and the temperature rise of cells under those conditions is studied. For an array of cells, the thermal model predicts significant

temperature rise along the airflow direction, suggesting the use of last cell temperature for thermal control. For short duration, high magnitude of current pulses, temperature rise is shown to be similar for same thermal energy deposited by different current pulses. The maximum thermal energy that can be deposited in the battery by a current pulse can be determined for given conditions of airflow rate, continuous current and air inlet temperature. The maximum magnitude of thermal energy that can be deposited by a peak current pulse to limit cell temperature is shown to be a function of current magnitude squared and the pulse duration time. For multiple current pulses applied to the battery pack, the model can evaluate the minimum time interval between current pulses to keep the temperature of cells within prescribed limits. The minimum time required between two current pulses is shown to decrease by increasing the airflow rate through the battery pack. By increasing the airflow rate, the battery pack is able to operate at a higher continuous current without exceeding the temperature limit.

Control-Oriented Thermal Model for a Hybrid Vehicle Battery

Rishit B. Modi

(GENERAL AUDIENCE ABSTRACT)

In a bid to reduce vehicular emissions, automobile manufacturers are moving towards electric and hybrid vehicles. Most hybrid vehicles have an energy storage system in addition to the conventional Internal Combustion (I.C.) engine. Lithium-ion batteries are used as energy storage systems in most hybrid vehicles due to their high energy density, long life and low self discharge rate. Lithium-ion batteries can be operated efficiently only in a narrow range of temperature. Operating these batteries outside of this temperature range results in their faster degradation which results in lower performance of hybrid vehicle. Due to this limitation, prevention of overheating in Lithium-ion batteries is extremely important. To keep the operation of Lithium-ion batteries within specified temperature limits, most batteries in hybrid vehicles are equipped with battery management systems (BMS). The BMS monitors cell voltage, cell temperature and applied current and keeps the temperature of cells within allowable limits. BMS of the battery pack used in this work has fan system for air-cooling the individual cells, and can lower the temperature rise of the cells by varying the fan speed. This BMS has limited temperature sensors that can predict surface temperature of few cells of the battery pack. Additional temperature information can be used to improve thermal control of the battery pack. This work presents a simplified thermal model that can be used in controller of a BMS to improve thermal control of cells and keep the temperature of cells within specified limits.

Dedication

I would like to dedicate this work to my parents, Bipin Modi and Shakuntala Modi.

Acknowledgments

I would like to thank Dr. Nelson for his guidance throughout two years of my graduate studies. I would like to thank all the sponsors of EcoCAR Mobility Challenge competition. Participation in this competition was a huge learning experience for me. Additionally, I would also like to thank all the team members of Hybrid Electric Vehicle Team at Virginia Tech for making two years of my life extremely memorable.

Contents

List of Figures

List of Tables

List of Symbols

$\dot{m}_{cell}$ Mass flow rate of air seen by a single cell

$\dot{m}_{fan}$ Mass flow rate of air coming from fan

μ_{air} Dynamic viscosity of air

ρ_{air} Density of air

A_{cell} Surface area of Lithium-ion cell

C_c Specific heat of cell core

$c_{p,air}$ Specific heat of air

C_s Specific heat of cell shell

D_{cell} Diameter of a single cell

h Convective heat transfer coefficient between air and cell

H_{cell} Height of a single cell

I Electric current

I_p Magnitude of current pulse

I_s Magnitude of continuous current

k_{air} Thermal conductivity of air

N_u Nusselt number for heat transfer between air and cell

P Gap between two cells

P_r Prandtl number for air

Q_c Heat conducted from battery core to shell

Q_{gen} Heat generated at cell core

Q_u Heat convected from battery core to shell

R_c Conduction resistance between cell core and shell

R_e Electrical resistance of a cell

T_c Temperature of cell core

$T_{f,i}$ Air temperature at cell i

T_s Temperature of cell surface

U_{inf} Free stream air velocity

U_{gap} Air velocity in gap between two cells

X_t Center to center distance between two cells in a pack

A_{busbar} Area of busbars used per cell

Chapter 1

Journal Paper

1.1 Introduction

In a bid to reduce automotive emissions, many automobile manufacturers in the world are developing either an electric or a hybrid vehicle running on both electricity and gasoline. Electric cars have higher efficiencies compared to conventional internal combustion (I.C.) engine cars. Conventional I.C. engine cars have 30 percent efficiency rate, compared to vehicles running on electricity that have 80 percent efficiency rate [1]

Electric vehicles are battery operated, with Lithium-ion batteries being the premier choice [3] due to high energy density, long life, and low self discharge rate [2] [4]. The performance of electric vehicles depends on the performance of the Lithium-ion battery being used, which strongly depends on the temperature range of operation [5] [6]. The optimum operating temperature for Lithium-ion cells lie in the range of $-20°C$ to $60°C$ [7]. A battery pack in a hybrid vehicle consists of many arrays of cells. When current is applied through the battery pack, the temperature of the cells rise. Cooling of the battery pack becomes necessary to keep the temperature of cells within operating limits. The battery pack being studied has a fan system for air-cooling the individual cells of the pack. The battery management system (BMS) monitors cell voltage, cell temperature and applied current and keeps the temperature of cells within allowable limits, by either changing the fan speed or communicating with the vehicle controller to adjust the charge/discharge current. The BMS used in the battery pack

has limited amount of temperature sensors which can predict the surface temperature of individual cells of the battery pack. Under extreme operating conditions, there is a $10°C$ difference in temperatures between the core and shell of the battery pack [8]. As a result, the surface temperature of cells is not representative of maximum cell temperature. Providing additional temperature information, such as the temperature of cell core, can help improve thermal control of the battery pack. The aim of this work is to develop a detailed thermal model, which can predict the core temperature of cells and can be used in a controller of BMS to keep the temperature of cells within allowable limits.

Thermal model of a cell consists of heat generation, accumulation and dissipation. Thermal models available in literature to simulate heat transfer in a battery pack can mainly be divided into 3 categories: lumped capacitance model, Finite Element Models, and 2- state models. Lumped capacitance model predicts only an average temperature throughout the cell. Since there is significant temperature gradient within a cell under extreme conditions, using a lumped capacitance model can cause under-prediction of the temperature rise of the battery pack, resulting in degradation of batteries. This limitation calls for a more accurate model, compared to lumped capacitance models. Finite Element Models [10] predict the detailed temperature distribution inside cells of battery packs. They are too complex to be implemented on a vehicle controller due to their high computation costs [11]. For the scope of this work, a 2-state model appears to be the best fit, since it can predict temperatures at cell interiors and surface, and can be implemented on a controller. [12] developed a model that predicts the battery core, surface and average temperatures using Hermite type integral approximations on energy equation. The reported results show that the average temperature of the cell is not representative of the core temperature of the cell, and is more representative of the battery shell. The analysis was carried out only for a single cell. Their thermal model provided reasonably accurate results for high values of Biot number (~ 1). [8] developed a

thermal model for a 26650 lithium-ion cell that can be used to predict the core temperature. The error between model and experiments were found to be below $1.5°C$. [8] [12] carried out the analysis only for a single cell in the battery pack. The model is yet to be validated for a battery pack consisting of many cells in series and parallel. The effect of bulk temperature rise of air as it moves downstream into the cell array is yet to be seen from a heat transfer standpoint. Changing the air mass flow rate inside the battery pack will result in a change in convection resistance. [8] assumed that convection resistance will remain constant, and its variation with mass flow rate was not studied. [9] used a 2-state model predicting the temperature at the core and shell of the battery pack. The analysis was carried out for moderate values of current ($0 \sim 50$ A), and the behaviour of the model under high current pulses is yet to be seen.

This work presents a thermal model that can predict the cell core temperature as a function of current applied. This information can be used to control the airflow rate from fan to keep the temperature of cells within allowable limits. This model is validated against limited experimental data available. The main objectives of this work are:

- Illustrate the temperature difference between core and surface of cell under high current pulses.
- Investigate the effect of bulk temperature rise of air on temperature rise of cells downstream in the pack.
- Investigate the maximum thermal energy that can be deposited in the battery pack by a single current pulse.
- Investigate the minimum time period required between multiple current pulses, so that the temperature of cells does not exceed $60°C$.

- Investigate the effect of changing airflow rate on the temperature rise of cells.

1.2 Modelling

1.2.1 Battery Pack layout

The battery pack being studied consists of 96 cells in series and 8 cells in parallel. Cells are connected in parallel to get higher Amp-hour capacity, and in series to get the desired voltage. Figure 1.1 shows the top view of cells arranged in a battery pack. The battery pack has 64 columns of 12 cells each. These 64 columns are divided into two layers, stacked one above the other. Samsung 18650 (diameter = 18.43 mm and height = 65mm) cells are used in the battery pack.

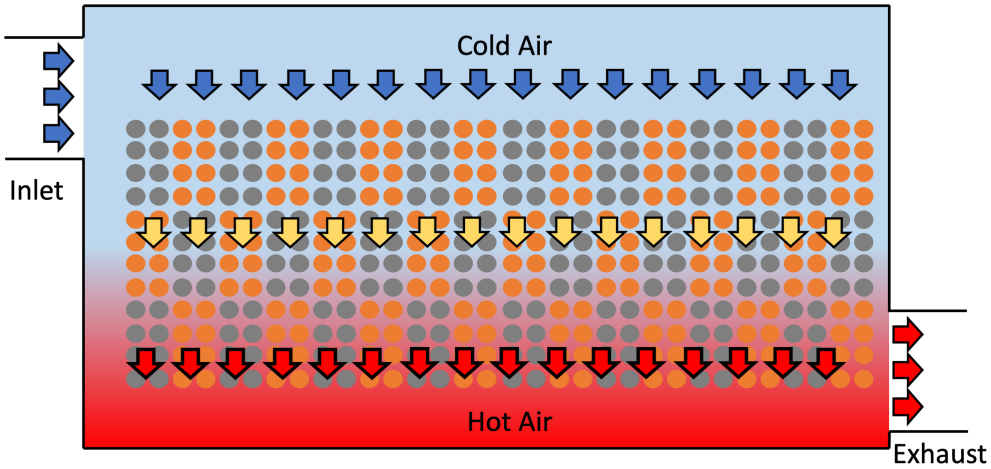

Figure 1.1: Layout of Battery Pack

The battery pack is entirely air cooled, and has 2 fans that are arranged in series to overcome the pressure drop across the pack. Vehicle cabin air enters the battery pack, and is being guided through a column of 12 cells. Due to cumulative heating from the cells, the temperature of air rises as it moves downstream into each column. The heated air is then exhausted

outside the vehicle. Figure 1.2 shows cells in a single layer in the battery pack. Based on the configuration of the pack, each of these 32 columns is assumed to receive the same amount of air flow. The temperature of cells, and that of air, is assumed to vary only in the direction of airflow, and there is no variation of temperature in the direction perpendicular to the airflow. The airflow rate, temperature of cells and air, are assumed to remain constant in a single row. Based on these assumptions, the analysis presented in the work is carried out for a single column of 12 cells. Due to uniform conditions in a single row, this analysis is valid for all 64 columns of the battery pack.

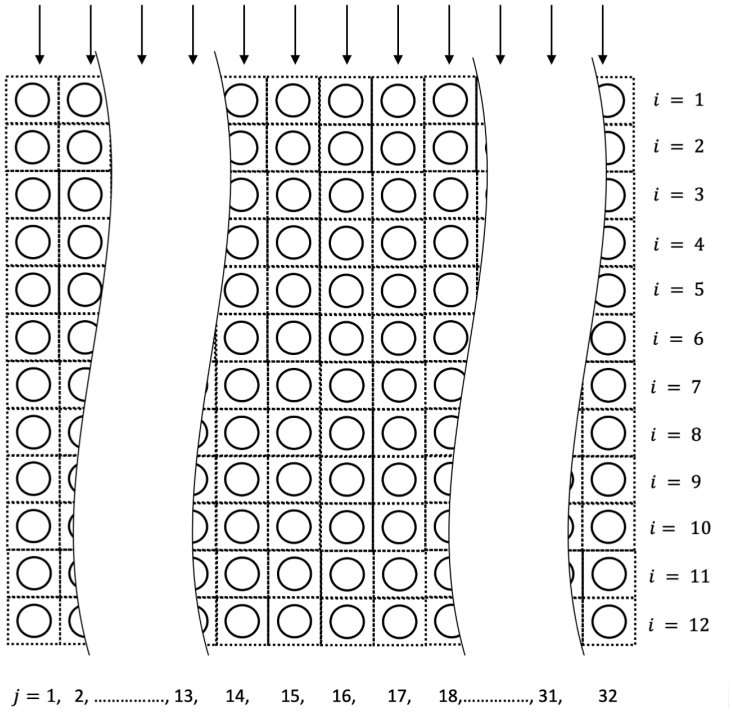

Figure 1.2: Top View of a Single Layer of Battery Pack

1.2.2 Thermal Model

Figure 1.3 shows an overview of the thermal model of an individual cell of the battery pack. Thermally, each cell is divided into two parts, viz. a core and a shell [11]. The core consists

of the cathode, anode and seperator, while shell consists of the outer casing of cell, which is made of steel. A conduction resistance R_c is used to model heat transfer between shell and the core of the cell. The shell is exposed to airflow on the outer surface and heat from the core on the inner surface. R_c can be estimated from the thermal conductivities of the cathode, anode, separator and the outer casing [11].

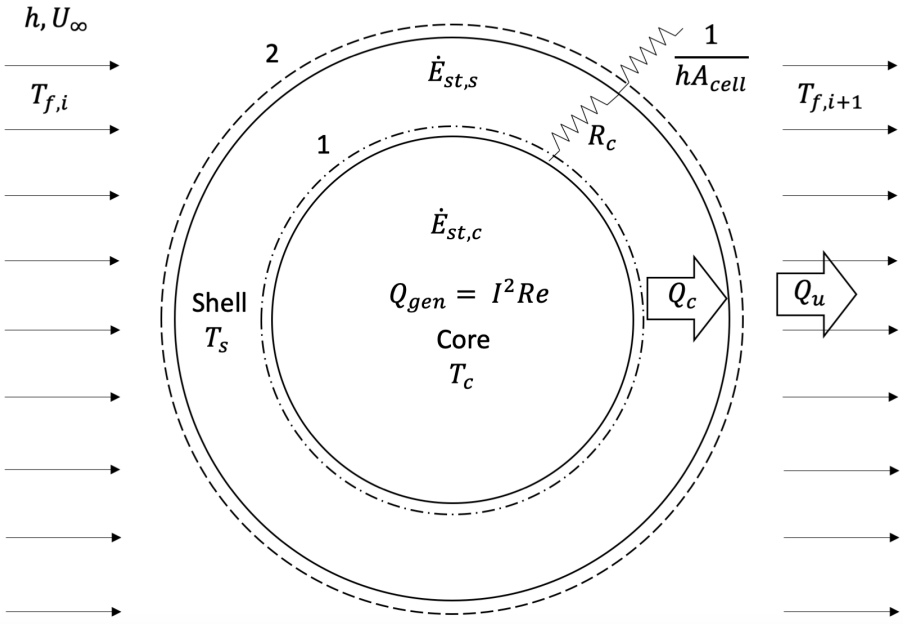

Figure 1.3: Thermal Model of a Single Cell.

Heat generation in lithium-ion cells consist of reversible (entropic) and irreversible heating (Joule loss). However, for applications of hybrid vehicles, the reversible heating is often neglected [12]. Application of current I through a cell results in a Joule loss of I^2R_e, where R_e represents the cell internal electrical resistance. All of this heat is assumed to be generated in the core of the cell. Q_{gen} in Figure 1.3 represents the energy generated in the core due to Joule heating. From Q_{gen}, Q_c gets conducted to the shell, while the rest $\dot{E}_{st,c}$ increases the temperature of core. Out of this Q_c heat, an amount equal to Q_u is convected to the airflow, and the rest $\dot{E}_{st,s}$ results in temperature rise of the shell. Heat transfer between shell and air is governed by a resistance $1/hA_{cell}$, where A_{cell} is the surface area of the cylindrical cell

and bus bars and h is the average value of the convective heat transfer coefficient across a column of 12 cells for turbulent flows. The following additional assumptions are made for the thermal model:

- The core and shell of all cells are assumed to be at a uniform temperature, T_c and T_s respectively.
- The thermal conductivity in the cell axial direction is an order of magnitude higher than the radial direction. The cell temperature is assumed to vary only in the radial direction.
- The temperature variation is small enough so that there is no variation of the air properties or the cell material heat capacities. The cell internal resistance is assumed to be constant at the average cell temperature and state of charge.

Energy balances at boundaries 1 and 2 for the cell give the following equations for the core and shell temperatures.

$$C_c \frac{dT_c}{dt} = Q_{gen} - Q_c \tag{1.1}$$

$$C_s \frac{dT_s}{dt} = Q_c - Q_u \tag{1.2}$$

$$\dot{m}_{cell} c_{p,air} \Delta T_f = h A_{cell} (T_s - T_f) \tag{1.3}$$

where,

$$Q_{gen} = I^2 R_e \tag{1.4}$$

$$Q_c = \frac{T_c - T_s}{R_c} \tag{1.5}$$

$$Q_u = hA_{cell}(T_s - T_f) \tag{1.6}$$

$$h = \frac{N_u D_{cell}}{k_{air}} \tag{1.7}$$

$$N_u = 0.27 {P_r}^{0.36} {R_{eD}}^{0.63} \tag{1.8}$$

$$R_{e,D} = \frac{\rho U_{gap} D_{cell}}{\mu_{air}} \tag{1.9}$$

where N_u, and hence h are obtained from [13]. C_c and C_s represent the heat capacities of the battery core and shell respectively. The shell heat capacity also includes the heat capacity of the bus bars being used in the battery pack. Reynold's number is based on the velocity of the air (U_{gap}) as it flows in the cell gap [13].

Air at free stream velocity U_∞ enters the battery pack. As air flows through a column of 12 cells, convective heat transfer between air and cells causes air temperature to rise from $T_{f,i}$ to $T_{f,i+1}$, where $i = 1, 2, 3, ...12$ is cell number in the column. This heat transfer results in higher temperature of air as it moves downstream in the array of 12 cells. Equations 1.1, 1.2, 1.3, 1.4, 1.5, 1.6 are discretized, based on time, using Euler explicit finite difference scheme and are solved for each of the 12 individual cells in a column. Table 1.1 lists the values of the parameters used in this work. Details of the methodology to estimate these parameters can be found in A.1.2. The values are given for a single cell of the battery pack.

Table 1.1: Parameters Used in the Model

Property	Value	Units
Core specific heat , C_c	30	$J/(Kg-K)$
Shell specific heat, C_s	12	$J/(Kg-K)$
Conduction Resistance, R_c	1.022	J/K
Internal Resistance, R_e	16.7	$mohm$

1.3 Model Validation

The validation of thermal model is carried out for two different cases. The cell temperature obtained from model data is validated against the values obtained from testing the battery pack. During testing, the temperatures were measured at the surface of cell 1 and cell 12. Table 1.2 gives the conditions for which the testing of battery pack was carried out.

Table 1.2: Conditions for Test Data

Property	Case 1	Case 2
Airflow rate	0 cfm	40.1 cfm
Air inlet Temperature	$19°C$	$19°C$
Initial Temperature - Cell 1	$19°C$	$22°C$
Initial Temperature - Cell 12	$19°C$	$48°C$
Battery Current	Variable	0 A

In Case 1, high charge/discharge current was passed through the battery pack during testing, and fans were kept shut off. Figure 1.4 shows a comparison of the model data with test data for cell 1. During testing, a maximum discharge current of 113 A, and a maximum charge current of 166 A is applied through the battery pack. In absence of any airflow, there is no difference in cell temperatures across 12 cells in a column. As a result, the model data is plotted just for the 1^{st} cell, and compared with test data of the 1^{st} cell. The maximum

temperature difference between model and test data is $2°C$. As seen from Figure 1.4, the cell temperature is overpredicted by the model at the end of current draw. The model presented in the paper does not account for natural-convection responsible for heat transfer in absence of any airflow. Additionally, there is a decrease in cell internal resistance R_e with increase in temperature, which has not been accounted for in the model. These factors result in a difference between model and test data.

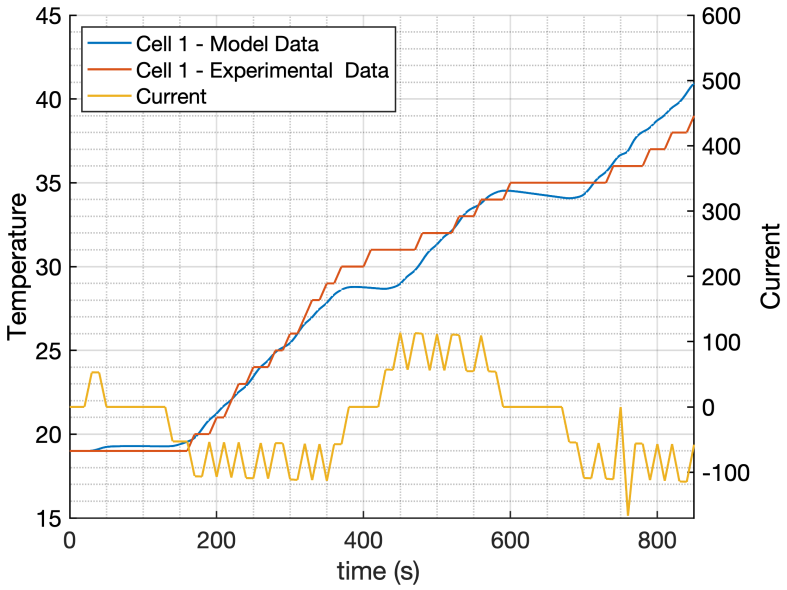

Figure 1.4: Validation for Case 1 Condition

Once the temperature of the cells reaches a high enough value, a cooldown test was performed on the battery pack in absence of any current. Light airflow (40.1 cfm) was used while performing cooldown test on the battery pack. Figure 1.5 shows a comparison between model data and test data.

In presence of airflow, there is a difference in temperatures between 12 cells of a column. The maximum temperature difference between model and test data is $1.5°C$, for cell 12. There is negligible difference between model data and test data for cell 1. The details of any uncertainty and errors in the measured data are unknown. Additionally, no information is

provided on where the temperature measurements are made, which can be accounted for the difference between measured and modelled cell temperatures.

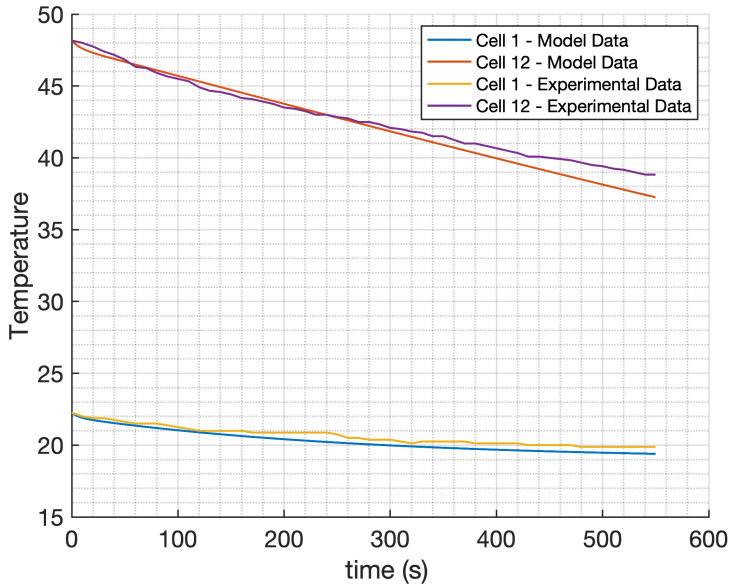

Figure 1.5: Validation for Case 2 Condition

1.4 Results and Discussion

Operating Lithium-ion batteries at a temperature above $60°C$ leads to faster cell degradation [7]. Under application of current, the temperature of individual cells of the battery rises up due to Joule heating. Hence, determining and monitoring cell temperature under various driving scenarios is important. The BMS functions to keep the cell temperature below $60°C$. Different current profiles are applied to the battery pack, and the cell temperature rise is studied. Impact of bulk temperature rise of air, and the effect of changing airflow rate is evaluated.

1.4.1 Single Current Pulse

Initially, a single current pulse is applied. Different combinations of parameters such as current applied, airflow rate, temperature of inlet air are chosen and two different cases are studied. Table 1.3 defines the values of the parameters for these cases. All current values represent the current applied through the entire battery pack of 96S8P configuration.

Table 1.3: Conditions for Single Current Pulse

	Case 1	**Case 2**
Airflow rate	40.1 cfm	40.1 cfm
Air inlet Temperature	$25°C$	$25°C$
Initial Temperature - Cell 1	$25°C$	$29°C$
Initial Temperature - Cell 12	$25°C$	$50°C$
Continuous Current	50 A	50 A
Current Pulse	-	250 A
Duration of Current Pulse	-	25 s

Figure 1.6 represents the steady-state temperatures achieved by the shell under Case 1 conditions. A current of magnitude 50 A is turned on at $t = 0$, for a time period of 4000 seconds. At $t = 4000$ s, the current is shut-off, and the cells are allowed to cool-down in presence of airflow. Temperature of each cell increases rapidly in response to the applied current, and reaches a steady-state value after a long enough time. Under steady-state conditions, the heat generated at the core, heat conducted from core to shell, and heat convected to air have the same magnitude. (i.e. $Q_{gen} = Q_c = Q_u$). Time required to reach steady-state conditions increases with increasing cell number. Time required to achieve steady-state condition for last cell is 3500 s, which is more than twice the time required for the 1^{st} cell. Figure 1.6 shows that the peak temperature achieved by the last cell is $50°C$, significantly higher compared to $30°C$ for the 1^{st} cell. This result can be explained by

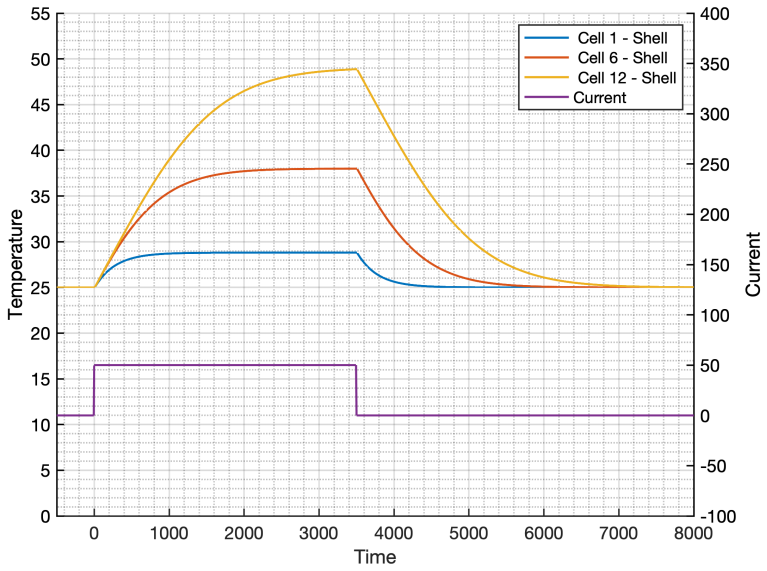

Figure 1.6: Steady State Temperatures Achieved by the Cells for Case 1 Condition

monitoring the bulk temperature rise of air.

Figure 1.7 shows the rise of bulk temperature during time $t = 0 - 3500$ s for cells 1-12. Initially, the bulk temperature of air is at $25°C$ for each cell. The bulk air temperature increases with time and cell number. Each cell generates heat at its core, which is conducted to the shell and dissipated via convection to the air. Cumulative heat from each cell causes higher air temperature with increasing cell number. As a result, the convection heat transfer for last cell is driven by a lower temperature difference. Since the value of heat transfer coefficient (h) and surface area are similar for all cells, a lower temperature difference means lower convective heat transfer rate for last cell. Under transient conditions, a significant portion of heat generated in the core of the last cell goes into increasing temperature of the last cell due to lower convective heat transfer, causing the last cell to have a higher temperature rise. This results in longer time to achieve steady-state for last cell, compared to cell 1. Once steady-state conditions are achieved, the convective heat transferred from each cell is same, and equal to I^2R_e heat generated in the cell core. Under steady-state

condition, bulk air temperature varies linearly with cell number.

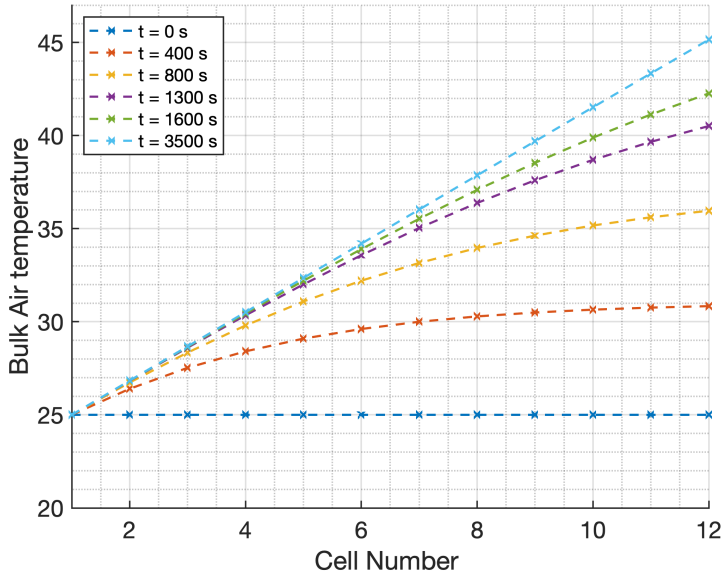

Figure 1.7: Rise of Bulk Air Temperature for Case 1 Condition

The current is shut-off at $t = 4000$ s, after which the temperature of cell starts decreasing due to airflow. Once current is shut-off, cell 12 takes 3000 s to reach back to initial conditions, as compared to 1000 s for cell 1. Figure 1.8 shows the variation of bulk air temperature over time after the current is shut-off.

Since the air temperature at last cell is higher compared to 1^{st} cell, last cell takes a longer time to cool-down to its initial conditions. At any time, the bulk temperature of air for last cell is higher than the 1^{st} cell. Last cell in the column sees the maximum temperature rise among all cells and hence, monitoring its temperature is important for the safe operation of battery pack. As this model helps determine the temperature of the last cell in the column, applying the model in a BMS would help the BMS to communicate with the vehicle controller when the temperature of the last cell rises above $60°C$. Based on the temperature of last cell, the BMS can also vary airflow rate so as to keep the temperature below $60°C$.

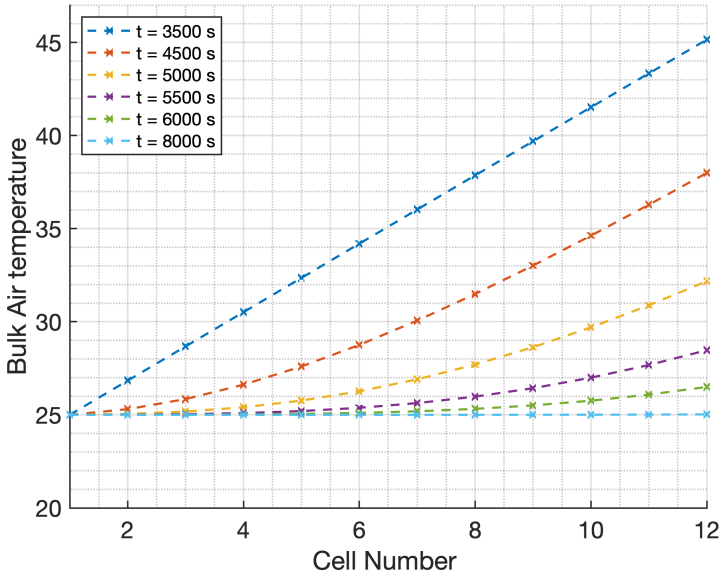

Figure 1.8: Fall of Bulk Air Temperature for Case 1 Condition

For Case 2 conditions, a current pulse of 250 A is applied on top of 50 A current. The pulse is applied after all the cells reach a steady-state temperature. The duration of pulse is 25 seconds. Figure 1.9 shows the temperature rise of cell 12 after application of current pulse of $250A$. There is a sharp increase in temperature due to rapid heat generation at core. At the time when core temperature reaches its peak value ($60°C$), the temperature of the core is $4°C$ higher than the shell. While the shell is within safe operating temperatures for Lithium-ion batteries, the core has exceeded the safety limit of $60°C$. Due to a finite conduction resistance between core and shell, the temperature of core always exceeds that of shell. This necessitates monitoring the core temperature, and keeping it below $60°C$.

Figure 1.10 shows a magnified view of Figure 1.9, between $t = 0 \sim 450s$. The spike in core temperature during that time interval can be explained as follows:

- When a high current pulse is applied, quite some portion of the heat generated at the core goes into thermal mass of the core, and the rest goes to shell via conduction,

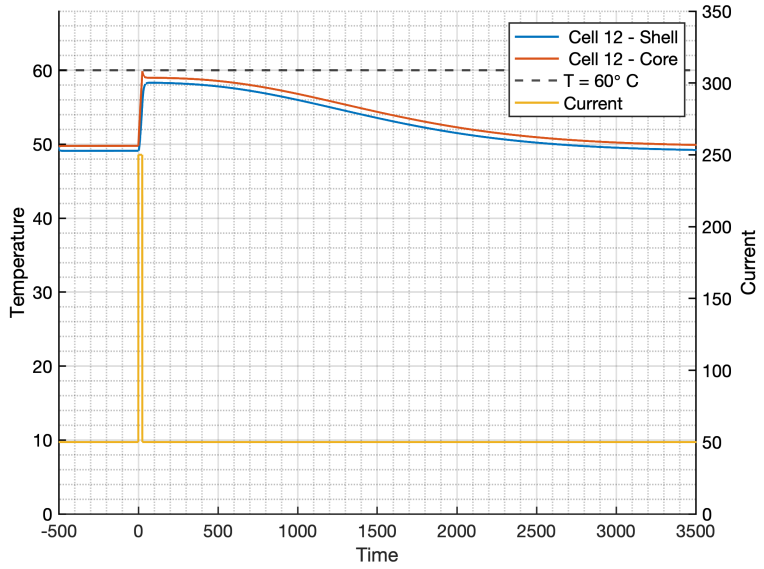

Figure 1.9: Cell Temperature Rise under Case 2 Condition

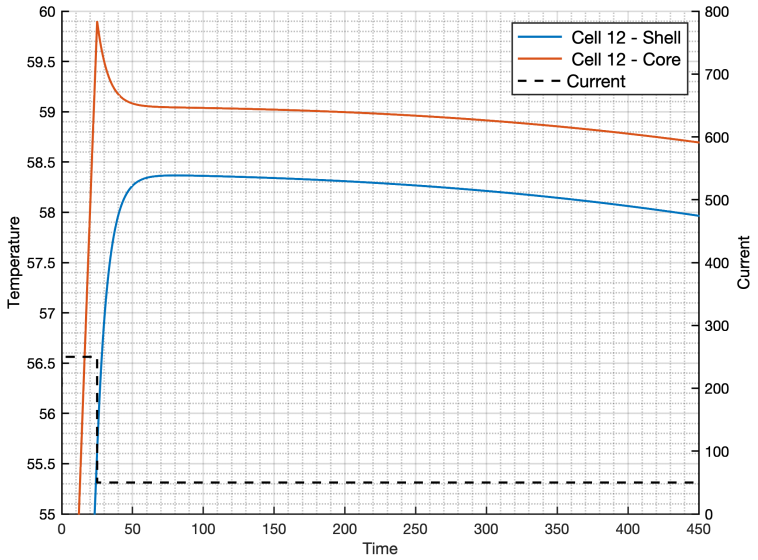

Figure 1.10: Zoomed View of Figure 1.9

resulting in higher temperature rise of the core compared to the shell. The temperature of the core at the end of the current spike is 60°C, while that of the shell is 56 °C.

- Once the current is shut off, the large temperature difference between core and shell,

combined with the fact that the conduction resistance is lower than the convection resistance ($R_c = 1.022$, compared with $1/(hA_{cell}) = 5.8$), results in sharp temperature drop from the core, while the shell temperature continues to rise.

- Shell temperature continues to rise, and reaches a maximum value, after which heat conduction from the core decreases due to lower temperature difference between core and shell. This causes a drop in the rate at which core temperature decreases.

1.4.2 Maximum Thermal Energy - $I^2R_e\Delta t$

The thermal energy of a current I applied to the pack for a period of Δt seconds is given by $I^2R_e\Delta t$, where R_e is the internal resistance.Figure 1.11 shows a current pulse of I_p applied on top of a steady current of I_s, for a time interval Δt. The additional thermal energy being deposited due to the current pulse I_p is $({I_p}^2 - {I_s}^2)R_e\Delta t$.

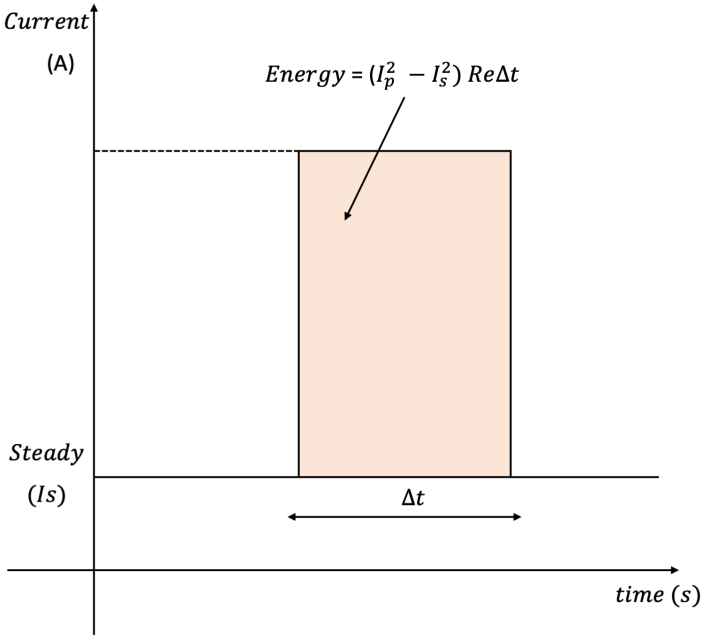

Figure 1.11: Thermal Energy Deposited by a Current Pulse I_p

Four cases with different values of current pulse and duration are chosen such that thermal

energy deposited in each case is the same. The temperature rise of the cells is studied for these 4 cases. Table 1.4 lists the conditions for which these cases are studied.

Table 1.4: Conditions for Current Pulses with Equal Thermal Energy

	Case 1	**Case 2**	**Case 3**	**Case 4**
Airflow Rate	40.1 cfm	40.1 cfm	40.1 cfm	40.1 cfm
Air Inlet Temperature	$25°C$	$25°C$	$25°C$	$25°C$
Initial Temperature - Cell 1	$29°C$	$29°C$	$29°C$	$29°C$
Initial Temperature - Cell 12	$50°C$	$50°C$	$50°C$	$50°C$
Continuous Current	50 A	50 A	50 A	50 A
Current Pulse	400 A	320 A	250 A	80 A
Duration of Pulse	9 s	15 s	25 s	385 s

Figure 1.12 shows the temperature rise of the cells under conditions of the above cases.

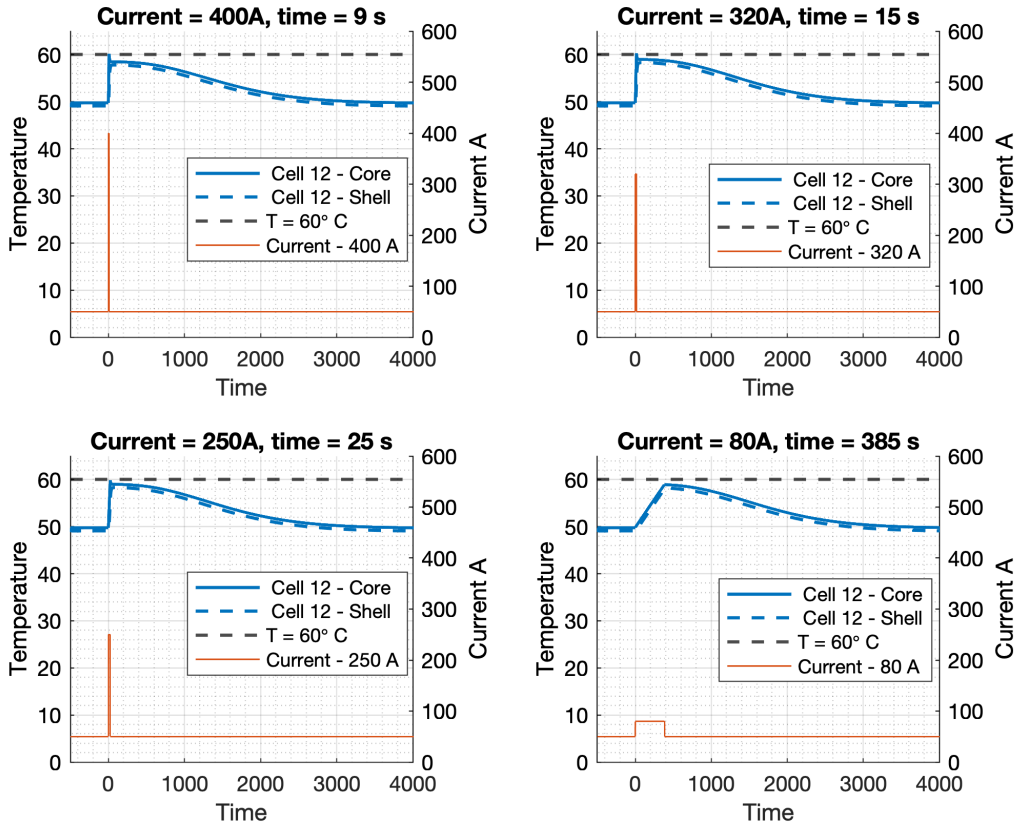

Figure 1.12: Cell Temperature Rise for Current Pulses having Equal Thermal Energy

All the cells are initialized from the steady state temperatures achieved after application of 50 A current. The thermal energy deposited in each of the above cases is equal to 300 kJ. The addition of 300 kJ of thermal energy causes the peak temperature of the last cell to be approximately equal to $60°C$ for each case. Table 1.5 represents the peak temperatures achieved by the cells in a column of the battery pack for these 4 different cases.

Table 1.5: Temperatures Achieved by Cells 1,6 and 12

Cell Number	Location	Case 1	Case 2	Case 3	Case 4
Cell 1	**Core**	$39.7°C$	$39.9°C$	$39.4\ °C$	$34.7°C$
	Shell	$35.9°C$	$36.3\ °C$	$36.2°C$	$33.2°C$
Cell 6	**Core**	$48.9°C$	$49.1°C$	$48.7\ °C$	$47.2\ °C$
	Shell	$46.5°C$	$47.0\ °C$	$47.0\ °C$	$46.2°C$
Cell 12	**Core**	$59.9\ °C$	$60.1\ °C$	$59.7°C$	$58.8°C$
	Shell	$58.1°C$	$58.2\ °C$	$58.2\ °C$	$58.1°C$

The peak temperatures of core and shell for the cells are approximately equal for each case. For Case 4, the temperatures are slightly lower when compared to the other 3 cases. Since the current pulse of $80A$ is applied for a relatively longer duration, more heat is transferred via convection, resulting in a lower temperature rise compared to the other 3 cases. A conclusion can be made that for short, high current pulses, the peak temperatures of the cells in the array are almost similar for equal amounts of thermal energy deposited. The maximum value of thermal energy that can be deposited in the battery pack varies with the continuous current applied, airflow rate, air inlet temperature. Since the core temperature of cell 12 has already reached $60°C$, the magnitude of the thermal energy $((I_p{}^2 - I_s{}^2)R_e\Delta t)$ deposited by the current pulse I_p should be less than 300 kJ for prescribed conditions. For known values of continuous current, airflow rate and air inlet temperature, the maximum thermal energy that can be deposited by a current pulse in the battery pack can be evaluated. Based on this value, a family of current pulses and duration that can keep the temperature of cells below

$60°C$ can be estimated. The feasibility of any current pulse can be determined by calculating the thermal energy deposited by the pulse. The maximum value of thermal energy can be used to set limits in the controller on the magnitude and duration of the peak current. This value allows the controller to keep the value of $({I_p}^2 - {I_s}^2)R_e\Delta t$ below the maximum limit of thermal energy that can be deposited for given conditions of airflow, continuous current and air inlet temperature.

1.4.3 Multiple Current Pulses

Under real driving scenarios, the current drawn by the vehicle controller should be feasible to keep the individual cell temperatures under 60 $°C$. The time period between two current pulses can be determined so that temperature of the last cell does not exceed $60°C$. Two current pulses are applied to the battery pack, and the temperature rise due to the current pulses is analyzed for 4 different time intervals between current pulses. Table 1.6 defines the conditions for which the test is carried out.

Table 1.6: Conditions for Minimum Time between Two Current Pulses

	Case 1	**Case 2**	**Case 3**	**Case 4**
Airflow Rate	40.1 cfm	40.1 cfm	40.1 cfm	40.1 cfm
Air Inlet Temperature	25	$25°C$	$25°C$	$25°C$
Initial Temperature - Cell 12	$50°C$	$50°C$	$50°C$	$50°C$
Continuous Current	50 A	50A	50 A	50 A
Magnitude of Single Current Pulse	250 A	250A	250 A	250 A
Duration of Single Current Pulse	15 s	15s	15 s	15 s
Time Period between Current Pulse	100 s	400 s	800 s	1100 s

Current pulse of $250A$ is applied after all cells reach a steady-state temperature after application of a continuous current of 50 A. Figure 1.13 shows the temperature rise of the cells

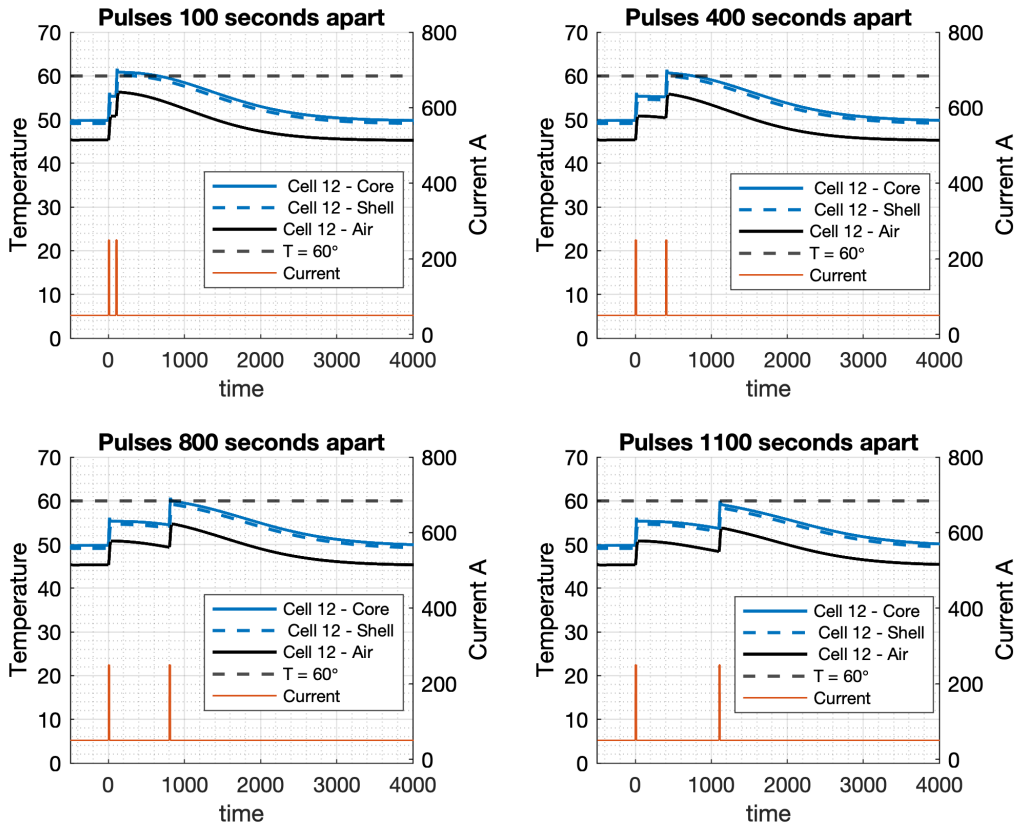

Figure 1.13: Temperature Rise for Two Current Pulses Seperated by Different Time Intervals

due to application of the current pulses. For Case 1,2 and 3, heat dissipated by convection during the time interval between two pulses is insufficient to lower the temperature significantly before the start of 2^{nd} pulse. For these cases, the bulk temperature of the air at the end of 1^{st} current pulse is relatively high, contributing to higher cell temperature. For Case 4, temperature of shell and core, as well as the air temperature is lowered sufficiently before the start of the 2^{nd} current pulse, resulting in temperature rise below $60°C$. Due to high thermal mass compared to convection heat transfer coefficient ($C_c/(hA_{cell}) = 190$), the temperature drop over a period of 1100 seconds is quite low ($\sim$1 °C). Increasing the airflow rate can reduce the minimum time period required between two current pulses significantly. This case of increasing the airflow rate is discussed in the next section. Since this model can

predict the minimum time period required between two current pulses, the model can help the BMS communicate with the vehicle controller so that the minimum time period can be kept to values such that the peak temperature rise is below $60°C$.

1.4.4 Control of Fan Speed

The effect of changing the airflow rate of fan on peak temperature rise of cells is studied. A temperature-based control is used wherein the airflow rate is increased after temperature of cells rise above a certain value. Reduction in minimum time required between two current pulses due to increase in airflow rate is demonstrated, for which conditions similar to Table 1.6 are used. The only difference is that instead of having air flow rate constant, the flow rate is increased from 40.1 cfm to 56.7 cfm when the temperature rises above $52°C$. Figure 1.14 represents the temperature rise of the cells under these conditions.

The temperature of the last cell is already below $60°C$, when the duration between the pulses is 800 seconds. The airflow rate is also shown in Figure 1.14. As soon as the temperature increases above $52°C$, there is a step change in airflow rate from 40.1 cfm to 56.7 cfm. Increasing the airflow rate causes minimum duration required between two pulses to decrease from 1100 seconds to 800 seconds.

Under steady-state conditions, the peak temperature of cell needs to be well below $60°C$, so that a current pulse can be accommodated. As shown in Figure 1.9, application of a current pulse of $250A$ for 25 seconds on top of a continuous current of 50 A results in the temperature of the last cell to rise to $60°C$. If a higher value of continuous current is desired, a pulse of $250A$ for 25 seconds would cause the temperature to rise well above $60°C$. The impact of increasing the mass flow rate on achieving a higher value of continuous current is analyzed for conditions given by Table 1.7.

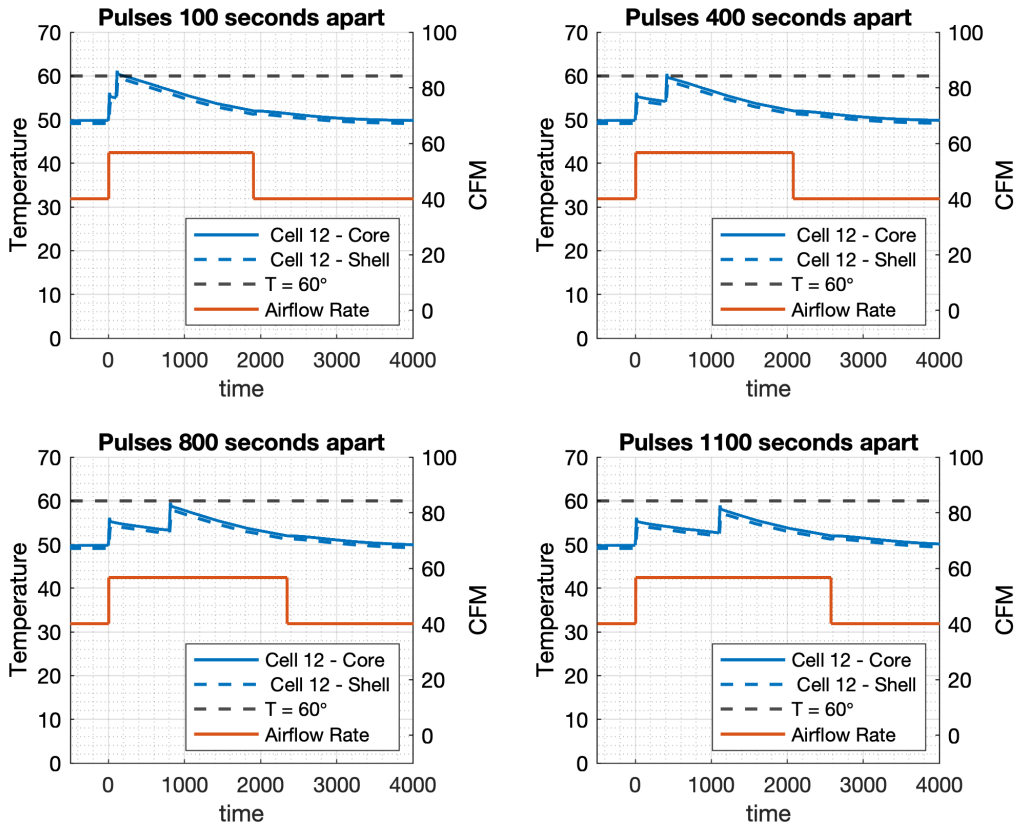

Figure 1.14: Temperature Based Control of Airflow Rate

Table 1.7: Conditions for Higher Continuous Current

	Case 1	**Case 2**
Airflow rate	40.1 cfm	59 cfm
Air inlet Temperature	$25°C$	$25°C$
Initial Temperature - Cell 1	$25°C$	$25°C$
Initial Temperature - Cell 12	$25°C$	$25°C$
Continuous Current	50 A	60 A
Current Pulse	250 A	250 A
Duration of Current Pulse	25 s	25 s

Figure 1.15 shows the temperature rise of the cells for Case 1 and Case 2 conditions. For Case 1 condition, with a continuous current of 50 A, the temperature of the last cell reaches $60°C$. For Case 2 condition, the continuous current is increased to 60 A, as a result of which the airflow has to be increased to 59 cfm so that the temperature rise can be limited to 60° C. A conclusion can be made that increasing the airflow rate can help to achieve a higher continuous current without exceeding the peak temperature of $60°C$, while still allowing for peak current pulses.

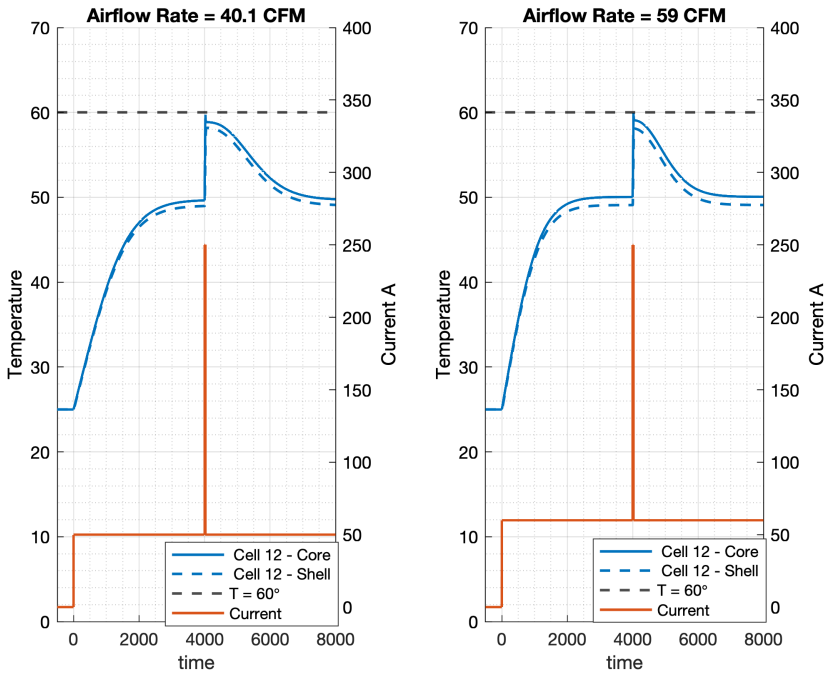

Figure 1.15: Impact of Airflow Rate on Achieving Higher Continuous Current

Depending upon the ambient conditions, there can be variation in the air inlet temperature and the initial cell temperature. For higher values of initial temperatures, the temperature rise of cells would be relatively higher, and the cell temperatures can exceed 60° C . Under such circumstances, the airflow rate can be varied to limit the temperature rise of the battery pack below $60°C$. For two different initial conditions, the impact of airflow rate on cell

temperature rise is analyzed for parameters defined by Table 1.8.

Table 1.8: Conditions for Higher Initial Temperature

	Case 3	**Case 4**
Airflow rate	40.1 cfm	51 cfm
Air inlet Temperature	30°C	30°C
Initial Temperature - Cell 1	30°C	30°C
Initial Temperature - Cell 12	30°C	30°C
Continuous Current	50 A	50 A
Current Pulse	250 A	250 A
Duration of Current Pulse	25 s	25 s

Figure 1.16 shows the temperature rise for Case 3 and Case 4. For Case 3, the peak temperature of the cell is 65°C, which is 5°C higher than Case 1 condition of Figure 1.15. The

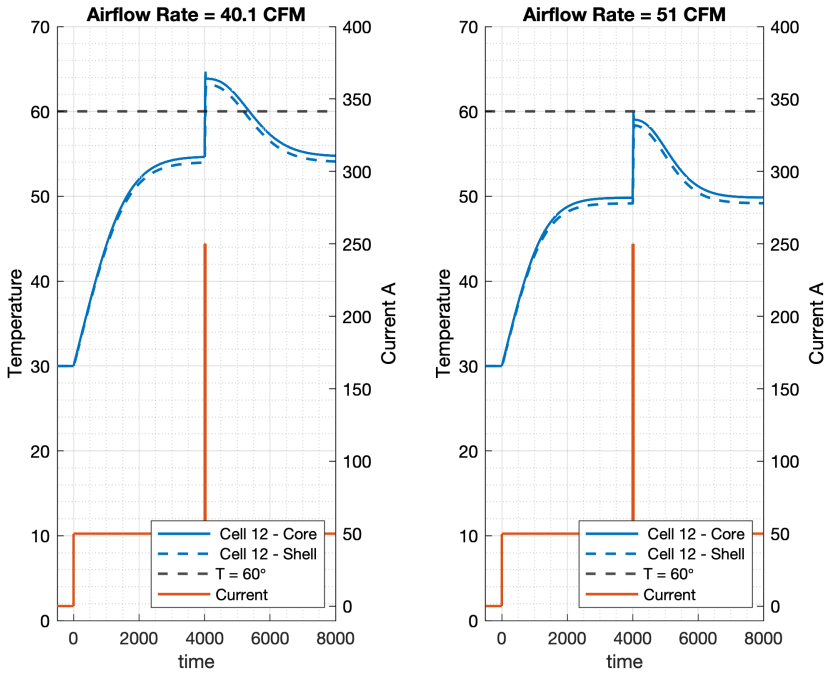

Figure 1.16: Impact of Airflow Rate on Higher Initial Temperature

airflow rate, continuous current and current pulse applied are similar between Case 3 in Table 1.8 and Case 1 in Table 1.7. The only difference between these cases is the initial condition. Both the cell initial temperature and air inlet temperatures are higher by $5°C$ for Case 3 compared to Case 1. For Case 4, airflow is changed from 40.1 cfm to 51 cfm, as a result of which temperature rise of the pack is limited to $60°C$. A conclusion can be made that for constant airflow rate and current applied, an increase in the initial temperature (say ΔT) will lead to same increase in peak cell temperature (ΔT). For higher values of initial temperatures, the airflow rate can be increased to limit the temperature rise below $60°C$.

1.4.5 Airflow Response

For implementation of thermal model in a controller, the drop in temperature over time needs to be analyzed for different airflow rates. Two different airflow rates are chosen and reduction in cell temperature over time is studied for conditions defined by Table 1.9.

Table 1.9: Conditions for Airflow Response

	Case 1	**Case 2**
Base Airflow Rate	40.1 cfm	40.1 cfm
Maximum Airflow Rate	50.1 cfm	60.1 cfm
Air Inlet Temperature	25° C	25° C
Initial Cell 1 Temperature	25° C	25° C
Initial Cell 12 Temperature	25° C	25° C
Continuous Current	59.2 A	59.2 A

For Case 1, the airflow rate of 40.1 cfm is applied initially. Once the cell 12 core temperature has reached steady-state temperature due to applied current of 59.2 A, the airflow rate is increased from 40.1 to 50.1 cfm while the current is held constant. Figure 1.17 represents the temperature variation under conditions of Case 1. The airflow rate as a function of time

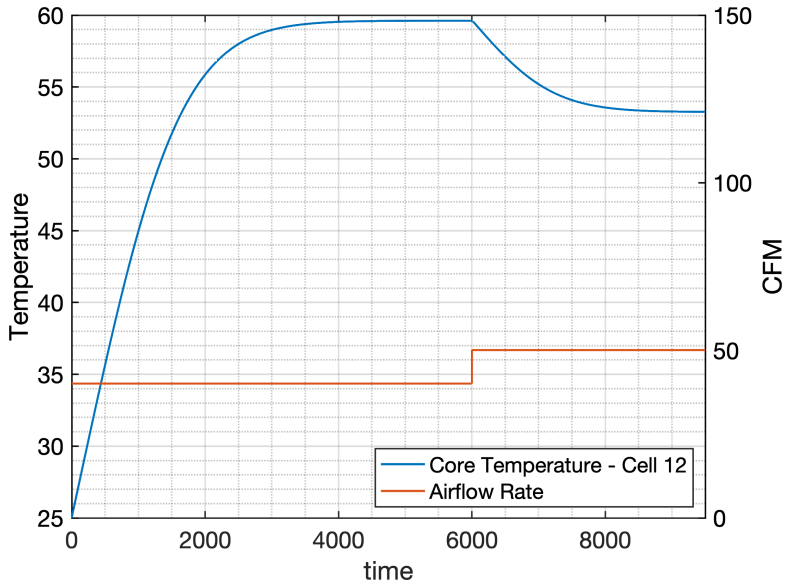

Figure 1.17: Temperature Rise for Case 1 of Airflow Response

is also shown. Due to current of magnitude 59.2A, the steady-state temperature of cell 12 has already reached 60°C. As a result, no current pulse can be accommodated on top of this continuous current of 59.2A. The airflow rate is then varied from 40.1 to 50.1 cfm resulting in decrease in temperature. This change in airflow rate causes the temperature of cell 12 core to reach a new steady-state value of 53°C. Time taken to achieve this new steady-state temperature is 3000 seconds.

Figure 1.18 represents the temperature rise under conditions of Case 2. For Case 2, all conditions are kept similar to Case 1 except the maximum airflow rate. The airflow rate is changed from 40.1 cfm to 60.1 cfm when steady-state temperature is achieved due to a constant current of 59.2A. After increasing the airflow rate, the temperature reaches a new steady-state of 49°C. The time taken to achieve a new steady-state temperature is 2500 seconds. Since a higher airflow rate is used for Case 2 compared to Case 1, the temperature drop is higher compared to Case 1. The time required to achieve steady-state conditions after changing the airflow rate is approximately 500 seconds less compared to Case 1. The

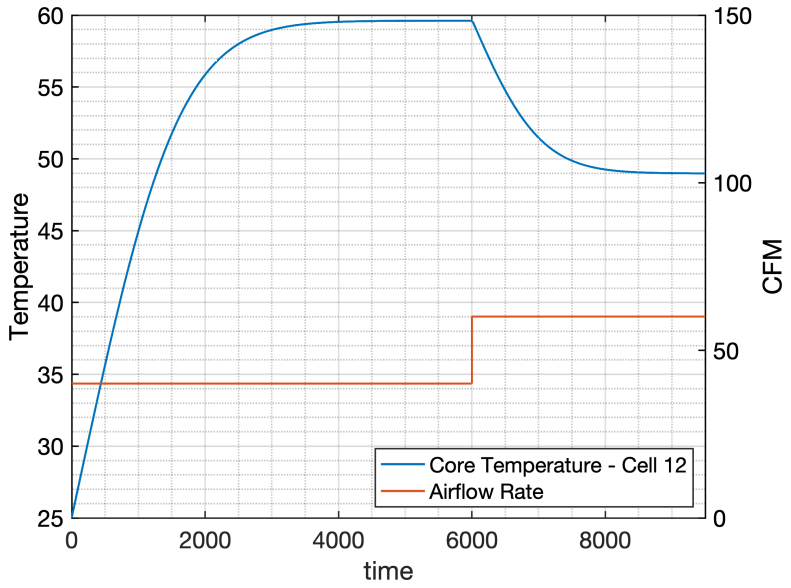

Figure 1.18: Temperature Rise for Case 2 of Airflow Response

faster temperature response and shorter time constant with constant heat generation are due to a higher convective heat transfer coefficient from higher airflow velocity.

1.4.6 Temperature Rise during a Drive Cycle

The temperature rise of the battery pack is studied over a US06 drive cycle. US06 is an aggressive drive cycle and the current trace obtained from US06 cycle is representative of a hybrid vehicle charge and discharge cycle under realistic driving conditions. Figure A.4 represents the velocity and acceleration trace of a US06 drive cycle. Figure 1.19 shows the predicted temperature rise of the core and shell over 4 consecutive US06 drive cycles. Two consecutive black lines indicate a single US06 drivecycle.

Airflow rate of 40.1 cfm is used. The cells are initialized at the steady-state temperatures achieved after applying 50 A current. The peak discharge current of the drivecycle is 237 A, while the peak charge current is 134 A. The temperature of the core and shell does not rise

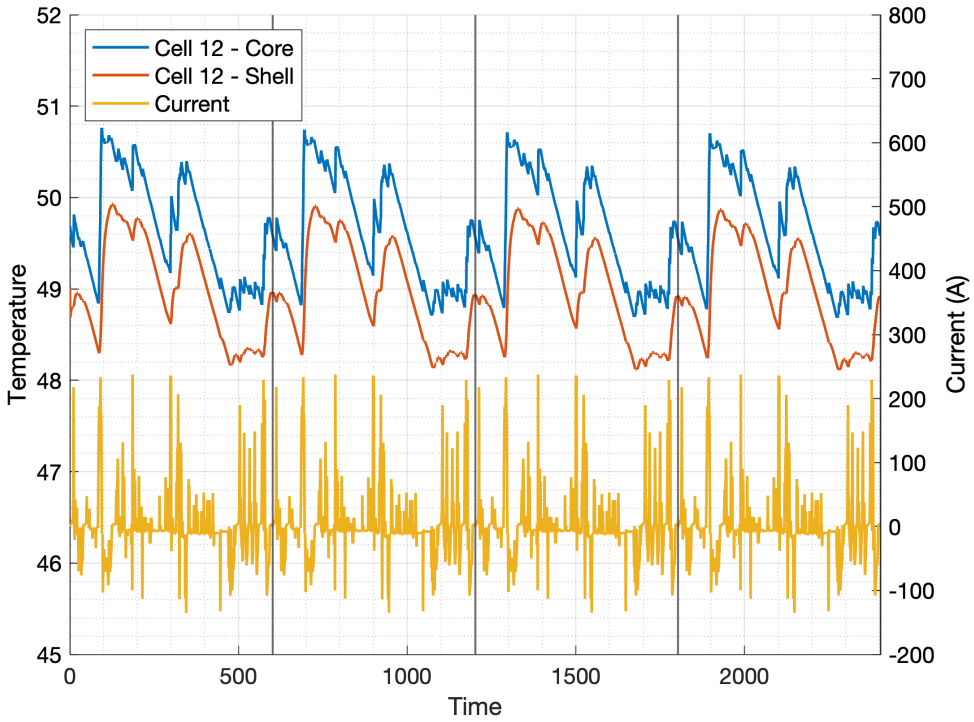

Figure 1.19: Temperature Rise over US06 Drive Cycle

drastically during the application of peak current due to high cell thermal mass as well as the short duration of peak current ($1 \sim 2$ seconds). The RMS current for this drive cycle is 50 A. Since the cells are also initialized at the steady-state temperatures achieved after applying 50 A current, quasi-steady state conditions are immediately achieved. Amount of I^2R_e heat generated by a steady current of 50 A is 41.75 W, which is approximately equal to the average heat generated during a single US06 drive cycle (41.61 W). A maximum difference of 2 $°C$ can be seen between the core and shell temperatures. The peak temperature achieved by the core is 50.7$°C$. This model can be used during development of a vehicle control strategy. For a given control strategy of a hybrid vehicle, this model can determine the peak temperature rise of the battery pack on a drive-cycle. Based on the temperature rise of battery pack, the control strategy can then be adjusted to meet the requirement of peak temperature to be

below $60°C$

1.5 Conclusion and Future Work

Lithium-ion batteries, used as energy storage systems in hybrid vehicles have an optimum operating temperature range between $-10°C$ and $60°C$. Higher magnitudes of applied current cause overheating of Lithium-ion batteries, resulting in faster degradation of the battery and consequently lower performance of the hybrid vehicle. Battery pack studied in this work has an air-cooled system. BMS used in the battery pack is equipped with limited temperature sensors for thermal control of the battery pack. Additional temperature information can be provided to the BMS to improve thermal control of the battery pack and consequently improve performance of the hybrid vehicle. To achieve this, a thermal model is created which can predict the core as well as the surface temperature of the cell for transient current conditions. Under extreme current pulses, there is significant temperature difference between core and surface of a cell. Since temperature sensors in BMS measure cell surface temperature, the measured temperature is not representative of the peak cell temperature. As a result, the thermal model presented in this work has sufficient fidelity to be used in BMS to improve real-time control of cell temperature. The model is validated against limited data available from testing of battery pack. For airflow across array of cells, a significant temperature rise occurs in the direction of airflow due to heat transfer from cells. The temperature rise is shown to be highest for the last cell in array and lowest for the 1^{st} cell. Cooling time required for last cell is shown to be significantly higher than the 1^{st} cell. Since last cell is representative of the peak temperature in the battery pack, control of parameters such as current and airflow rate should be based on the core temperature of the last cell. For short duration, high magnitude current pulses, the peak temperature rise of the cells is shown to be similar

for equal amounts of thermal energy deposited in the pack. The maximum value of thermal energy that can be deposited in the battery pack by a given current pulse can be evaluated for known values of continuous current applied, airflow, and the air inlet temperature. A given peak current pulse magnitude and duration can limit the temperature rise below $60°C$ if the thermal energy deposited by the pulse is below the maximum limit for those conditions. As a result, a separate analysis need not be carried out for different values of peak current pulse and duration. The maximum magnitude of thermal energy that can be deposited by a peak current pulse to limit cell temperature is shown to be a function of current magnitude squared and the pulse duration time. This model can be used to set limits on the magnitude and duration of the current pulse in a controller so that the cell temperature remains within allowable limits. The model is then used to determine the minimum time period required between two current pulses to keep the temperature rise below $60°C$. A temperature-based control of airflow is depicted and a conclusion is made that increasing the airflow rate based on temperature of cells can reduce the minimum required time interval between two current pulses. Increasing the airflow rate can be used to operate the battery pack at a relatively higher continuous current without exceeding $60°C$. Increase in air inlet temperature and cell initial temperature by a magnitude ΔT is shown to increase the peak cell temperature by the same magnitude, ΔT. For higher cell initial and air inlet temperatures, increasing the airflow rate is used to limit the temperature rise below $60°C$. The model is applied to a US06 drive cycle to predict the temperature rise and the battery pack is shown to be able to perform a US06 drive cycle without exceeding the threshold temperature of $60°C$.

Suggestions for future work include:

- Validation of the thermal model for different values of airflow rate and current applied across the battery pack.

- Number of cells in the flow direction have significant effect on the temperature rise of the last cell, the heat transfer coefficient h, and the pressure drop across cell array. Decreasing the cell gap will increase the heat transfer coefficient as well as the pressure drop across the battery pack by making the pack more compact. A sensitivity study can be conducted to determine the effect of cell gap on the peak temperature rise of the cells.

- Conducting a sensitivity to determine the effect of various parameters on the air outlet temperature. Based on the measured air outlet temperature by the temperature sensors in the BMS, the parameters affecting the air exit temperature can then be adjusted in the model to obtain a better estimate of cell temperature.

- Value of cell internal resistance changes with time. Variation of cell internal resistance can be incorporated in the model to improve model fidelity with pack ageing.

Appendix

Appendix A

A.1 Supplemental Material

A.1.1 Modelling of Control Volume

Since the battery packs consists of two layers of cells, the incoming airflow is assumed to be equally distributed among the two layers. Furthermore, in a single layer of the battery pack, the airflow is assumed to equally divide among 32 rows of 12 cells. Figure A.1 shows a control volume surrounding the individual cells of the battery pack.

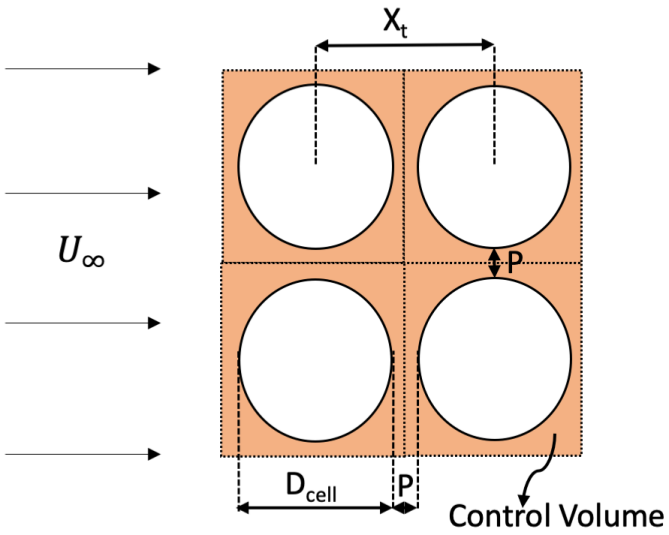

Figure A.1: Control volume Used in the Model

The total airflow received by the starting cell of the row is given by:

$$\dot{m}_{cell} = \frac{\dot{m}_{fan}}{64} \tag{A.1}$$

The center to center distance X_t between two cells is given by:

$$X_t = D_{cell} + P \tag{A.2}$$

where P is the gap between two cells and D_{cell} is the cell diameter. The area of the control volume (A_{cv}) for one cell is given by:

$$A_{cv} = X_t H_{cell} \tag{A.3}$$

where H_{cell} is the cell height. The face velocity of air, as seen by a single cell is given by

$$U_{inf} = \frac{\dot{m}_{cell}}{\rho_{air} A_{cell}} \tag{A.4}$$

where ρ_{air} is the density of air. The velocity in the cell gap is given by

$$U_{gap} = \frac{U_{inf} X_t}{X_t - D_{cell}} \tag{A.5}$$

U_{gap} is used to calculate the Reynold's number. The surface area (A_{cell}), through which convection heat transfer occurs, is given by

$$A_{cell} = \pi D_{cell} H_{cell} + A_{busbar} \tag{A.6}$$

where, A_{busbar} indicates the surface area of the busbars per cell. The bus bars are assumed to have good electrical and thermal contact with cells, and are assumed to be at the same temperature as shell.

Table A.1 represents physical properties of cell, as well as thermal properties of air used in the model.

Table A.1: Properties Used in the Model

Property	Value
Cell mass, m	48 gram
Cell diameter, D_{cell}	18.43 mm
Cell height, H_{cell}	65 mm
Cell pitch, P	3.015 mm
Cell center to center distance, X_t	21.445 mm
Air specific heat, c_p	1.005 $kJ/(kg-K)$
Air viscosity, μ	1.85×10^{-5} m^2/s
Prandtl number, P_r	0.72
Thermal conductivity of air, k_{air}	0.025 $W/(m-K)$
Specific heat of bus bars, C_{busbar}	1.2 (J/K)
Bus bar material	Cu_{110} Alloy
Bus bar area per cell	460 mm^2

A.1.2 Estimation of Parameters

The value of specific heat of Samsung 18650 cells is obtained from [14]. The material of the cell casing is steel. From the thickness of cell casing and specific heat of steel (510 $J/(kg-K)$), the specific heat of shell is estimated at 10 $J/(kg-K)$. The value of core specific heat is obtained by subtracting the cell specific heat from the shell specific heat. Value of R_c is obtained by using the thermal conductivity of cell obtained from [15].

A.1.3 Analytical Solution

The governing equations for the shell and core temperatures 1.1 and 1.2 can be solved analytically for a single cell. The analytical solution to these equations are given by:

$$T_c = c_1 e^{\lambda_1 t} + c_2 e^{\lambda_1 t} + k_1 \tag{A.7}$$

$$T_s = c_3 e^{\lambda_1 t} + c_4 e^{\lambda_1 t} + k_2 \tag{A.8}$$

where,

$$\lambda_1 = \frac{-a + \sqrt{a^2 - 4b}}{2} \tag{A.9}$$

$$\lambda_2 = \frac{-a - \sqrt{a^2 - 4b}}{2} \tag{A.10}$$

The coefficients a, and b are given by:

$$a = \frac{1}{C_c R_c} + \frac{1}{C_s R_c} + \frac{h A_{cell}}{C_s} \tag{A.11}$$

$$b = \frac{h A_{cell}}{C_c C_s R_c} \tag{A.12}$$

The constants k_1 and k_2 are given by:

$$k_1 = T_{f,i} + I^2 R_e R_c + \frac{I^2 R_e}{h A_s} \tag{A.13}$$

$$k_2 = T_{f,i} + \frac{I^2 R_e}{hA_s} \tag{A.14}$$

where $T_{f,i}$ represents the inlet bulk temperature of the air. c_1 and c_2 are constants depending on the initial conditions.

For an array of 12 cells, the bulk air temperature also varies from cell to cell. As a result, a numerical scheme is used to solve the governing equations 1.1 and 1.2. An Euler explicit finite difference method is used in order to discretize the governing equations.

$$C_c \frac{T_c(i,k+1) - T_c(i,k)}{\delta t} = Q_{gen} - Q_c \tag{A.15}$$

$$C_s \frac{T_s(i,k+1) - T_s,(i,k)}{\delta t} = Q_c - Q_u \tag{A.16}$$

where,

$$Q_c = \frac{T_c(i,k) - T_s(i,k)}{R_c} \tag{A.17}$$

$$Q_u = hA_{cell}(T_s(i,k) - T_f(i,k)) \tag{A.18}$$

$$Q_u = \dot{m} c_p (T_f(i+1,k) - T_f(i,k)) \tag{A.19}$$

where $i = 1, 2, ...12$ represents the discretization based on cell number, and k represents the

discretization based on time.

Figure A.2 shows a comparison between the analytical and numerical solutions. The analytical and numerical simulations are conducted for conditions of case 1 in Table 1.3. Initial transient effects cause a minor difference in core temperatures between the numerical and analytical solution, after which it reduces to zero.

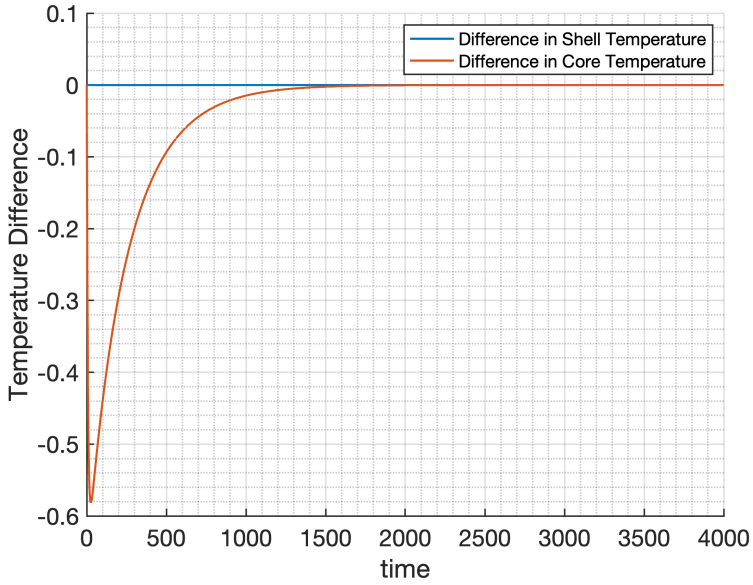

Figure A.2: Comparison between Analytical and Numerical solution

For all the studies, a time step (dt) of 1 second is used. Under conditions of case 1 of Table 1.3, the stability of solution is verified. A comparison between time step $dt = 1$ second and $dt = 0.01$ second is shown in Figure A.3. The error in temperature for time steps $dt = 1s$ and $dt = 0.01s$ is less than 0.014 percent. A conclusion can be made that changing the time step results in negligible change in solution, and the finite difference scheme employed is stable for $t \leq 1$ seconds.

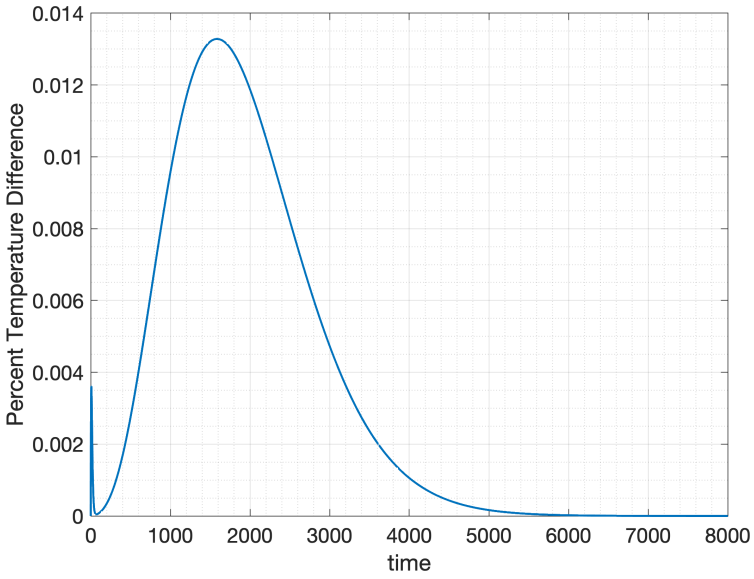

Figure A.3: Comparison between Time Steps

A.1.4 US06 drive cycle

The US06 drive cycle is a 8.01 mile route, with a top speed of 35.8 m/s , average speed of 21.6 m/s, and a duration of 596 seconds. Figure A.4 shows the velocity trace of a US06

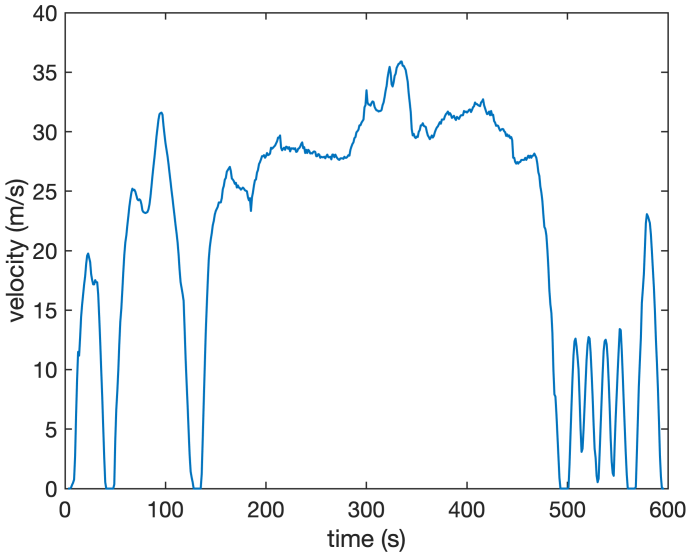

Figure A.4: Velocity Trace of US06 Drive Cycle

drivecycle.

A.1.5 Maximum thermal energy

For a steady current of 50 A, the maximum thermal energy that can be deposited by the current pulse is evaluated for different flow rates. Figure A.5 shows the maximum thermal energy that can be deposited by the current pulse as a function of the airflow rate. The maximum flow rate for the fans in the battery pack is 145.7 cfm. Initially, the maximum thermal energy that can be deposited in the battery pack rises sharply with increase in airflow rate. After a certain thermal energy is deposited in the pack, increase in the airflow rate results only in a slight increase in the maximum value of thermal energy that can be deposited by the current pulse. The maximum thermal energy that can be deposited in the pack without exceeding $60°C$ is 850 kJ, for airflow rate 145 cfm.

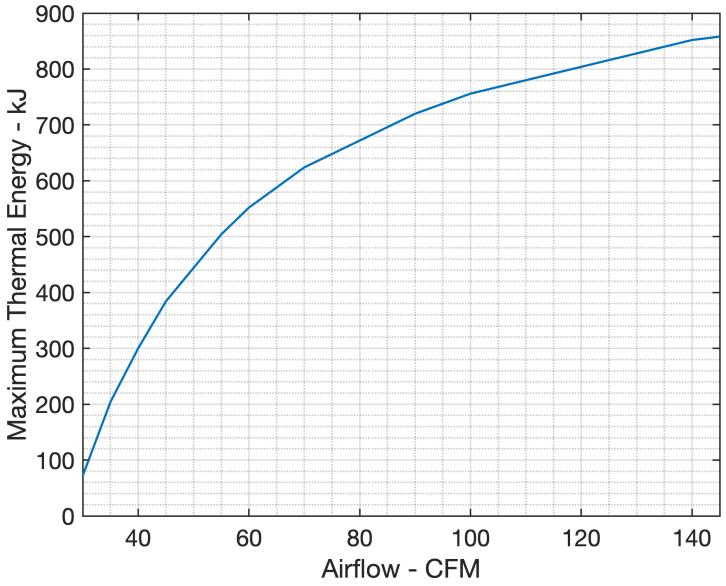

Figure A.5: Maximum Thermal Energy Deposited in the Pack

References

[1] Silverstein, K., 2020. What's Driving The Move To Electric Vehicles?. [online] Forbes. Available at: https://www.forbes.com/sites/kensilverstein/2016/10/13/whats-driving-the-move-to-electric-vehicles/285c0bd35fb7 [Accessed 23 April 2020].

[2] Thanagasundram, S., Arunachala, R., Makinejad, K. and Jossen2, A., 2012. A Cell Level Model for Battery Simulation. In: European Electric Vehicle Congress. pp.1-13.

[3] Benger, R., Wenzl, H., Beck, H., Jiang, M., Ohms, D. and Schaedlich, G., 2009. Electrochemical and thermal modeling of lithium-ion cells for use in HEV or EV application. World Electric Vehicle Journal, 3(2), pp.342-351.

[4] Jeon, D. and Baek, S., 2011. Thermal modeling of cylindrical lithium ion battery during discharge cycle. Energy Conversion and Management, 52(8-9), pp.2973-2981.

[5] Parsan, A. and Keyser, M., 2001. Thermal characteristics of selected EV and HEV batteries. In: Sixteenth Annual Battery Conference on Applications and Advances. IEEE, pp.219-225.

[6] Vignesh, B., Grandjean, T., McGordon, A. and Greenwood, D., 2018. Thermal Modeling Of Lithium Ion Batteries For Temperature Rise Predictions In Hybrid Vehicle Application. In: Thirteenth International Conference on Ecological Vehicles and Renewable Energies (EVER). Institute of Electrical and Electronics Engineers (IEEE).

[7] Väyrynen, A. and Salminen, J., 2012. Lithium ion battery production. The Journal of Chemical Thermodynamics, 46, pp.80-85.

[8] Forgez, C., Vinh Do, D., Friedrich, G., Morcrette, M. and Delacourt, C., 2010. Thermal modeling of a cylindrical LiFePO4/graphite lithium-ion battery. Journal of Power Sources, 195(9), pp.2961-2968.

[9] Park, C., and Jaura, A. K., 2003. Dynamic Thermal Model of Li-Ion Battery for Predictive Behavior in Hybrid and Fuel Cell Vehicles. SAE Technical Paper Series, 2003-01-2286.

[10] Ma, Y., Teng, H. and Thelliez, M., 2010. Electro-Thermal Modeling of a Lithium-ion Battery System. SAE International Journal of Engines, 3(2), pp.306-317.

[11] Xinfan Lin, Perez, H., Siegel, J., Stefanopoulou, A., Yonghua Li, Anderson, R., Yi Ding and Castanier, M., 2013. Online Parameterization of Lumped Thermal Dynamics in Cylindrical Lithium Ion Batteries for Core Temperature Estimation and Health Monitoring. IEEE Transactions on Control Systems Technology, 21(5), pp.1745-1755.

[12] Mahamud, R. and Park, C., 2013. Spatial-resolution, lumped-capacitance thermal model for cylindrical Li-ion batteries under high Biot number conditions. Applied Mathematical Modelling, 37(5), pp.2787-2801.

[13] Žukauskas, A., 1972. Heat Transfer from Tubes in Crossflow. Advances in Heat Transfer, Volume 8, pp.93-160.

[14] Yayathi, S., Walker, W., Doughty, D. and Ardebili, H., 2016. Energy distributions exhibited during thermal runaway of commercial lithium ion batteries used for human spaceflight applications. Journal of Power Sources, 329, pp.197-206.

[15] Bhundiya, H., Hunt, M. and Drolen, B., 2018. Measurement Of The Effective Radial Thermal Conductivities Of 18650 and 26650 Lithium Ion Battery Cells. In: Thermal and Fluid Analysis Workshop, NASA Jet Propulsion Laboratory. Galveston.